Physics Letters A 393 (2021) 127185

Contents lists available at ScienceDirect

Physics Letters A

www.elsevier.com/locate/pla

Extension of finite-strain equations of state to ultra-high pressure

Roman Tomaschitz

Sechsschimmelgasse 1/21-22, A-1090 Vienna, Austria

ARTICLE INFO

Article history:
Received 29 October 2020
Received in revised form 6 January 2021
Accepted 19 January 2021
Available online 22 January 2021
Communicated by L. Ghivelder

Keywords:
Ultra-high pressure equation of state (EoS) for solids
Eulerian and Lagrangian finite-strain expansions
Compression modulus and free energy
Broken power-law densities
Least-squares regression of the EoS of copper
Birch-Murnaghan EoS

ABSTRACT

Eulerian and Lagrangian finite-strain expansions are extended into the ultra-high pressure range by way of an isothermal closed-form EoS, a broken power-law density depending on four parameters determined by least-squares regression. The EoS is put to test with high-pressure data sets of copper up to 60 TPa and can be used to extrapolate data sets obtained in the GPa range to ultra-high densities approaching the Thomas-Fermi free-electron regime. In the low and intermediate pressure range up to a few hundred GPa, the EoS admits finite-strain ascending series expansions, which coincide with the third-, fourth- and fifth-order Birch-Murnaghan and Lagrangian EoSs, subject to the finite-strain expansion parameter used. The pressure evolution of the compression modulus of copper is obtained from the regressed EoS. A closed-form expression of the free energy over the full pressure range up to the Thomas-Fermi limit is derived and compared with finite-strain theory.

1. Introduction

The aim is to find an equation of state (EoS) for solids that is applicable in the ultra-high pressure regime and also reproduces finite-strain EoSs in the low and intermediate pressure range, such as the third- and fourth-order Birch-Murnaghan EoSs or EoSs based on the Lagrangian finite-strain expansion. To this end, we introduce a four-parameter broken power-law density as high pressure EoS, and put it to test with high- and ultra-high pressure data sets of copper, using shockless compression data up to 450 GPa [1] and a data set obtained from DFT calculations covering pressures up to 60 TPa [2]. The parameters of the EoS are determined by least-squares regression, using the compression modulus at zero-pressure and its derivative as input parameters obtained from low-pressure ultrasonic measurements [3–5].

Based on the regressed high-pressure EoS of copper, we determine the pressure evolution of the compression modulus as well as the density dependence of the free energy of copper, which can be obtained in closed form and remains applicable at ultra-high pressure. The high-pressure asymptotics of the EoS and its relation to the Thomas-Fermi free-electron limit is discussed as well. We then perform a finite-strain ascending series expansion of the broken power-law EoS and the associated free energy, using Eulerian and Lagrangian finite-strain expansion parameters. We demonstrate that the third-, fourth- and fifth-order Birch-Murnaghan EoSs (in the case of an Eulerian expansion) and the corresponding Lagrangian EoSs can be recovered in this way, as well as other finite-strain EoSs defined by a general finite-strain exponent α, see below. The proposed EoS is thus an extension of finite-strain EoSs (which are truncated series expansions) into the high pressure and density regimes.

This paper is organized as follows. In Section 2.1, the high-pressure EoS is introduced, a four-parameter EoS that is a broken power-law density in density-versus-pressure representation $\rho(P)$. The associated compression (bulk) modulus $K(P)$ and its derivatives at zero pressure are derived. In Section 2.2, we use high-pressure data sets of copper extending up to 60 TPa and discuss least-squares regression of the broken power-law EoS. In particular, we explain how to use this EoS to extrapolate low- and intermediate-pressure data sets into the ultra-high pressure Thomas-Fermi regime.

In Section 3, the relation of the broken power-law EoS to finite-strain theories, cf. e.g. Refs. [6–13], is studied, based on the finite-strain expansion parameter $f=-\varepsilon/(3\alpha)$, $\varepsilon=(\rho/\rho_0)^\alpha-1$, where ρ_0 denotes the density at zero pressure and α is the finite-strain exponent. Eulerian finite-strain expansions require the exponent $\alpha=2/3$, leading to Birch-Murnaghan EoSs, and Lagrangian finite-strain EoSs are defined by $\alpha=-2/3$. In Section 3.1, we invert the broken power-law EoS $\rho(P)$ to obtain the pressure-versus-density representation $P(\rho)$, and then perform an ascending series expan-

E-mail address: tom@geminga.org.

https://doi.org/10.1016/j.physleta.2021.127185
0375-9601/

sion thereof in powers of ε, which can be done without specifying the finite-strain exponent α. In Section 3.2, this epsilon expansion is shown to lead to the third-, fourth- and fifth-order Birch-Murnaghan and Lagrangian EoSs, depending on how many orders in ε are taken into account and on the choice of α. In this way, we demonstrate that the broken power-law EoS is effectively a summation of truncated series expansions in ε. In contrast to EoSs based on finite-strain expansions, the proposed closed-form EoS remains applicable at high- and ultra-high pressure. We also use the high-pressure EoS of copper, obtained from a least-squares fit in Section 2.2, to illustrate the very limited pressure range (up to a few hundred GPa) in which Eulerian and Lagrangian finite-strain expansions can be used.

In Section 4.1, we derive the free energy of copper by integrating the broken power-law EoS inferred by least-squares regression. The free energy calculated in this way is applicable over the full pressure range, covering the crossover from the low to the ultra-high pressure regime. In Section 4.2, an ascending series ε expansion of the free energy is performed, from which the finite-strain EoSs discussed in Section 3 (such as the Birch-Murnaghan and Lagrangian EoSs) can be derived. Finally the Eulerian and Lagrangian finite-strain ε expansions of the free energy of copper are compared with the free energy obtained from the regressed closed-form EoS. Section 5 contains the conclusions.

2. High-pressure equation of state as broken power-law density

2.1. Compression modulus and its derivatives

The isothermal EoS discussed in this paper is a broken power-law density in $\rho(P)$ (density-versus-pressure) representation,

$$\frac{\rho(P)}{\rho_0} = \frac{1}{(1+(a/b)^{\beta/\eta})^\eta}\left(1+\left(\frac{a+P}{b}\right)^{\beta/\eta}\right)^\eta, \tag{2.1}$$

with positive fitting parameters a, b, β, η. Asymptotically, $\rho(P\to 0)\sim\rho_0$ and $\rho(P)\propto P^\beta$ in the opposite high-pressure regime, and the amplitudes a, b and exponent η determine the crossover between these two power-law limits, which appear as straight lines in log-log plots of density $\rho(P)$. Similar (multiply) broken power-law densities have been used to model heat capacity data of crystals [14,15]. These densities are quite efficient to analytically reproduce, via least-squares regression, the fine-structure of data sets extending over several logarithmic decades [16]. ρ_0 in (2.1) denotes the mass density at zero (i.e. ambient) pressure; zero-pressure values will be indicated by a subscript zero. The first ratio in (2.1) is just a normalization constant, so that $\rho(P\to 0)/\rho_0\sim 1$. The second factor is structurally similar to the (inverted) Murnaghan EoS $\rho(P)/\rho_0=(1+PK_0'/K_0)^{1/K_0'}$, cf. e.g. Ref. [17], where K_0 denotes the bulk modulus $K(P)$ at zero pressure and K_0' its pressure derivative. The Murnaghan EoS is thus a special case of EoS (2.1) with $a=0$, $b=K_0/K_0'$ and $\beta=\eta=1/K_0'$. The parameter a has no counterpart in the Murnaghan EoS, but is essential to make the EoS (2.1) analytic at zero pressure, since the exponent β/η (to be inferred from a least-squares fit) is non-integer. In the low-pressure regime, the EoS (2.1) is equivalent to finite-strain EoSs (such as the third- and fourth-order Birch-Murnaghan EoSs), as will be demonstrated in Section 3. The closed-form EoS (2.1) is thus an extension of finite-strain series expansions into the high pressure range.

The compression modulus based on EoS (2.1) reads

$$K(P)=\frac{\rho(P)}{\rho'(P)}=\frac{1}{\beta}(a+P)\left(1+\left(\frac{a+P}{b}\right)^{-\beta/\eta}\right), \tag{2.2}$$

and admits the ascending series expansion $K(P)=K_0+K_0'P+K_0''P^2/2+K_0^{(3)}P^3/6+\cdots$, with zero-pressure coefficients

$$K_0=\frac{a}{\beta}\left(1+(a/b)^{-\beta/\eta}\right),\qquad K_0'=\frac{1}{\beta}+(a/b)^{-\beta/\eta}\frac{\eta-\beta}{\eta\beta}, \tag{2.3}$$

$$K_0''=(a/b)^{-\beta/\eta}\frac{\beta-\eta}{a\eta^2},\qquad K_0^{(3)}=(a/b)^{-\beta/\eta}\frac{\eta^2-\beta^2}{a^2\eta^3}. \tag{2.4}$$

Eqs. (2.3) can be solved for the amplitudes a and b,

$$a=K_0\frac{\eta-\beta}{K_0'\eta-1},\qquad b=K_0\frac{\eta-\beta}{K_0'\eta-1}\left(\frac{\eta(1-K_0'\beta)}{\beta-\eta}\right)^{\eta/\beta}, \tag{2.5}$$

so that

$$a/b=\left(\frac{\eta(1-K_0'\beta)}{\beta-\eta}\right)^{-\eta/\beta},\qquad 1+(a/b)^{\beta/\eta}=\frac{\beta(1-K_0'\eta)}{\eta(1-K_0'\beta)}. \tag{2.6}$$

We can then substitute (2.5) and (2.6) into (2.4) to find

$$\begin{aligned} K_0''&=\frac{(1-K_0'\beta)(1-K_0'\eta)}{\eta K_0(\beta-\eta)},\\ K_0^{(3)}&=\frac{(K_0'\beta-1)(K_0'\eta-1)^2(\beta+\eta)}{\eta^2K_0^2(\beta-\eta)^2}. \end{aligned} \tag{2.7}$$

The first of these equations can be solved for β, which is substituted into the second to arrive at

$$\begin{aligned} \beta&=\frac{1-K_0'\eta+K_0K_0''\eta^2}{K_0'(1-K_0'\eta)+K_0K_0''\eta},\\ K_0^{(3)}&=\frac{K_0''+(2K_0K_0''-K_0'^2)K_0''\eta^2}{\eta K_0(K_0'\eta-1)}. \end{aligned} \tag{2.8}$$

The second of these equations is quadratic in η and solved by

$$\begin{aligned} \eta_\pm&=\frac{K_0K_0^{(3)}\pm R}{2(K_0'^2K_0''-2K_0K_0''^2+K_0K_0'K_0^{(3)})},\\ R&:=\left(4K_0'^2K_0''^2-8K_0K_0''^3+4K_0K_0'K_0''K_0^{(3)}+K_0^2K_0^{(3)2}\right)^{1/2}. \end{aligned} \tag{2.9}$$

In this way, we can express the fitting parameters a, b, β, η in Eq. (2.1) by the compression modulus at zero pressure K_0 and its derivatives $K_0^{(n=1,2,3)}$. In fact, substituting $\eta_\pm$ into (2.8) gives $\beta_\pm$, and substitution of $\eta_\pm$ and $\beta_\pm$ into (2.5) gives $a_\pm$ and $b_\pm$ as functions of $K_0^{(n=0,1,2,3)}$.

The correspondence $(a,b,\beta,\eta)\leftrightarrow(K_0,K_0',K_0'',K_0^{(3)})$, made explicit here is not one-to-one. First, all parameters (a,b,β,η) in the EoS (2.1) have to be positive, which puts constraints on the $K_0^{(n=0,1,2,3)}$. Conversely, positivity of K_0' imposes a constraint on (a,b,β,η), see the second equation in (2.3). Finally, one set of parameters $K_0^{(n=0,1,2,3)}$ can correspond to two sets of $(a_\pm,b_\pm,\beta_\pm,\eta_\pm)$ or one set or none, depending on whether the latter are positive, cf. (2.9).

The EoS (2.1) is a phenomenological EoS that can be traced back to finite-strain expansions, cf. Section 3, and does not make assumptions on interatomic potentials. The four fitting parameters of EoS (2.1) are related to the compression modulus and its derivatives at zero pressure, which are measurable quantities by way of low-pressure ultrasonic experiments. Typically, K_0 and K_0' are known from acoustic measurements, so that only two independent fitting parameters remain in EoS (2.1), which can be regressed from high-pressure data sets. The derivatives K_0'' and $K_0^{(3)}$ can then be calculated from the regressed parameters, as exemplified in Section 2.2 with data sets of copper.

Table 1
Input and fitting parameters of the closed-form EoS of copper at ambient temperature of 300 K. The broken power-law EoS $\rho(P)$ used for the fit is defined in (2.1) with amplitudes a, b in (2.5) substituted. The compression modulus K_0 at zero pressure and its derivative K_0' obtained from ultrasonic measurements [3] are taken as input parameters, cf. Section 2.2. The fitting parameters are the exponents β and η in EoS (2.1); the least-squares fit is depicted in Fig. 1. Also recorded are the minimum of the least-squares functional $\chi^2=\sum_{i=1}^N(\rho(P_i)-\rho_i)^2/\rho_i^2$ and the degrees of freedom (dof: number N of data points (P_i,ρ_i) minus number of fitting parameters). The data sets are referenced in the caption of Fig. 1. The standard error of the χ^2 fit, $\mathrm{SE}=(\sum_{i=1}^N(\rho(P_i)-\rho_i)^2/N)^{1/2}$, and the determination coefficient, $R^2=1-\sum_{i=1}^N(\rho(P_i)-\rho_i)^2/(N\sigma^2)$, with sample variance $\sigma^2=\sum_{i=1}^N(\rho_i-\bar\rho)^2/N$ and mean $\bar\rho=\sum_{i=1}^N\rho_i/N$, are listed as well.

K_0 [GPa]	K_0'	β	η	χ^2	dof	SE	$1-R^2$
133.5	5.36	0.45901	1.3949	1.17×10^{-3}	$116-2$	0.0145	1.73×10^{-4}

2.2. Least-squares regression of the EoS of copper

The broken power-law EoS (2.1) is non-perturbative and can also be used at ultra-high pressure. A practical way to perform a least-squares fit over an extended pressure range is to eliminate the amplitudes a, b in EoS (2.1) by substituting (2.5) and (2.6) into the EoS, so that $\rho(P)/\rho_0$ only depends on two fitting parameters β and η, provided that K_0 and K_0' are known input parameters. In case that also the second derivative K_0'' is known from acoustic experiments, one can eliminate β by substituting (2.8) into the EoS, so that there is only one fitting parameter η left.

If only K_0 is known, one can use K_0',β,η as fitting parameters, typically with $K_0'\approx5$ as initial guess, cf. e.g. Refs. [3–5]. Alternatively, one can solve the first equation in (2.3) for b, $b=a(K_0\beta/a-1)^{\eta/\beta}$, to be substituted into the EoS (2.1), so that a, β, η are fitting parameters and K_0 is experimental input. Finally, there is the option to use EoS (2.1) as it stands for least-squares regression, and to determine K_0 and its derivatives from the fitting parameters (a,b,β,η) by way of (2.3) and (2.4).

The high-pressure asymptotic limit of EoS (2.1) and the compression modulus (2.2) reads

$$\frac{\rho(P)}{\rho_0}\sim\frac{(P/b)^\beta}{(1+(a/b)^{\beta/\eta})^\eta},\qquad K(P)\sim\frac{P}{\beta},\tag{2.10}$$

from which one can obtain an initial guess for the exponent β by fitting a power law (which appears as straight-line in log-log plots) to high-pressure data. Also, $K_\infty':=K'(P\to\infty)=1/\beta$. For comparison, the EoS $\rho(P)\propto P^{3/5}$ of a non-relativistic degenerate electron gas (Thomas-Fermi free-electron limit [6,11]) gives $K_\infty'=5/3$, so that $\beta=3/5$. Phenomenological thermodynamic arguments were used in Refs. [18,19] to suggest the inequality $K_\infty'>5/3$ instead of $K_\infty'=5/3$ advocated in Ref. [6], which implies the constraint $\beta<3/5$ on this exponent, although this is not a necessary equilibrium condition. The fact that the material will undergo structural transitions [19] does not exclude the Thomas-Fermi limit either. If discontinuities emerge in the empirical density-pressure curve partitioning the pressure range into intervals, one has to perform a least-squares fit of (2.1) in each of the intervals. Whether $K_\infty'>5/3$ or $K_\infty'=5/3$ applies in the high-pressure limit is ultimately to be decided empirically; both options will be studied here.

In Figs. 1 and 2, we consider two high-pressure data sets for copper: a data set up to 450 GPa, obtained by shockless compression [1], which is extended to 60 TPa with data points from DFT calculations [2], all at ambient temperature. Ultrasonic estimates of K_0 and K_0' [3–5] are used as input parameters, cf. Table 1. The EoS (2.1) with (2.5) substituted then depends on two fitting parameters, the exponents β and η. The least-squares fit is depicted in Fig. 1, the fitting and goodness-of-fit parameters are listed in Table 1. The pressure dependence of the compression modulus is also depicted in this figure, as well as the Murnaghan EoS, which is determined by the input parameters K_0 and K_0' alone. Once the exponents β and η are known, one can calculate the amplitudes a, b in the EoS via (2.5), as well as the second- and third-order derivatives of the compression modulus by way of (2.7), which are listed in Table 2. We find $K_\infty'=1/\beta\approx2.18$, so that the constraint $K_\infty'>5/3$ mentioned above is satisfied.

Table 2
Parameters derived from the least-squares fit of the broken power-law EoS (2.1) of copper. The χ^2 fit is described in Fig. 1 and Table 1 and Section 2.2. Recorded are the amplitudes a, b in EoS (2.1), calculated via (2.5) with fitting parameters in Table 1. K_0'' and $K_0^{(3)}$ denote the second- and third-order pressure derivatives of the compression modulus $K(P)$ at zero pressure and ambient temperature, calculated via (2.4), which define the expansion coefficients (3.8) of the finite-strain approximations to the EoS. The amplitudes a, b and exponents β, η (see Table 1) completely determine the EoS (2.1) and its inversion (3.1), the latter being the starting point of the finite-strain expansions in Sections 3.2 and 4.2. ρ_0 is the ambient (zero-pressure) density of copper.

a [GPa]	b [GPa]	K_0'' [1/GPa]	$K_0^{(3)}$ [1/GPa^2]	ρ_0 [g/cm^3]
19.291	205.03	-5.427×10^{-2}	3.739×10^{-3}	8.939

In Fig. 2, we perform a one-parameter fit of EoS (2.1) (with amplitudes (2.5) substituted), using K_0, K_0' and the exponent $\beta=3/5$ as input parameters and η as fitting parameter, assuming the Thomas-Fermi limit $K_\infty'=5/3$ in the ultra-high pressure regime instead of the constraint $K_\infty'>5/3$. First, we perform a fit of the same data sets (up to 60 TPa) as in Fig. 1. The density-pressure curve obtained in this way is depicted as solid red curve in Fig. 2, and the fitting and goodness-of-fit parameters are recorded in Table 3. The goodness-of-fit parameters are, of course, worse than those of the two-parameter fit of the same data set in Table 1.

In Fig. 2, we also perform a second one-parameter fit, with the same input parameters K_0, K_0' and β, but discard the ultra-high pressure data obtained from DFT calculations. That is, in the χ^2 functional (cf. the caption of Table 1), only the experimental data (up to 450 GPa) are included. The fit obtained in this way is depicted in Fig. 2 as blue solid curve, and the fitting and goodness-of-fit parameters are listed in Table 4. For comparison, we have also indicated, in linear-log representation, the two-parameter fit discussed in Fig. 1, which is shown as green solid curve.

In case that the second derivative K_0'' of the bulk modulus is also known from ultrasonic measurements, the exponent η can be obtained by solving the first equation in (2.8) instead of using least-squares regression, so that all parameters of EoS (2.1) are determined by specifying $K_0^{(n=0,1,2)}$ and $\beta=3/5$. The least-squares fits depicted in Figs. 1 and 2 will be further discussed in Section 5.

We study the EoS (2.1) of copper at ambient temperature, for lack of high-pressure data at high temperature. The four fitting parameters in EoS (2.1) are actually temperature-dependent functions $a(T)$, $b(T)$, $\beta(T)$, $\eta(T)$, to be inferred by least-squares regression. To this end, one needs isothermal pressure-density measurements taken at a sequence of temperatures T_n. A least-squares fit of EoS (2.1) can then be performed to each of these pressure isotherms,

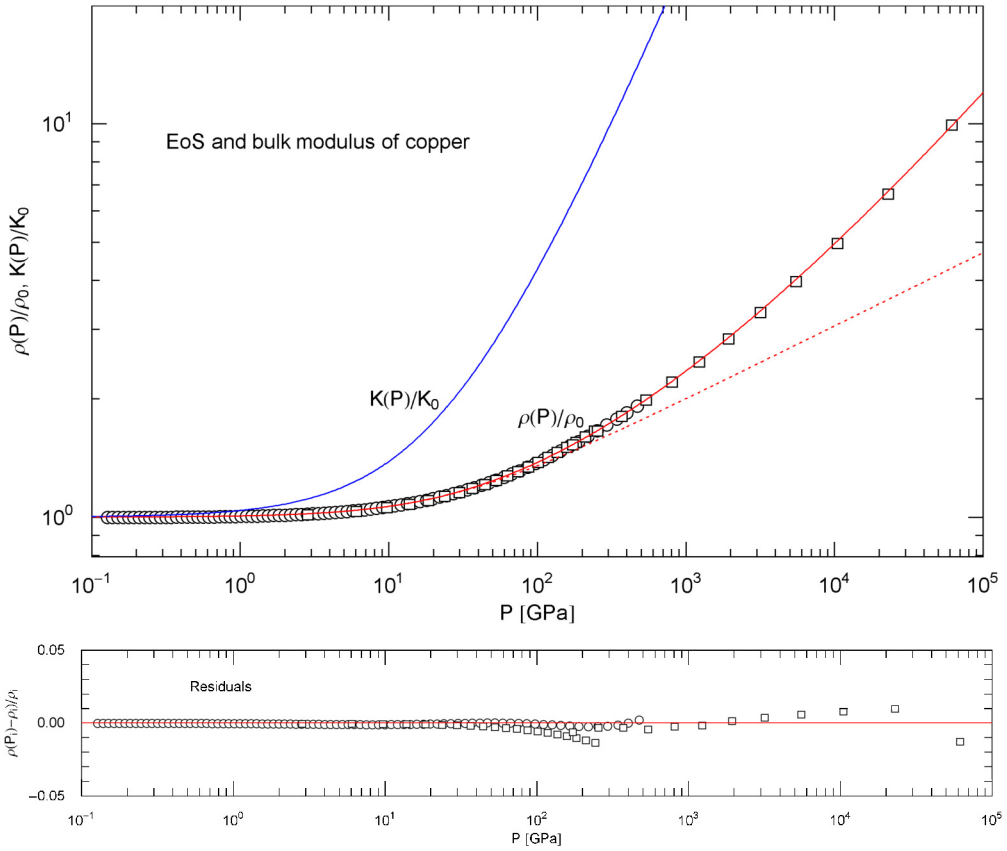

Fig. 1. EoS and compression modulus of copper at ambient temperature. Data points up to 450 GPa (circles) obtained by shockless compression [1] and up to 60 TPa (squares) from DFT calculations [2]. The two-parameter χ^2 fit (solid red curve) is performed with the EoS $\rho(P)$ defined in (2.1) (with amplitudes a, b in (2.5) substituted). The fitting parameters are the exponents β and η in EoS (2.1); the compression modulus K_0 at zero pressure and its derivative K_0' are taken as input from low-pressure acoustic experiments, cf. (2.5) and Table 1. The blue solid curve shows the compression modulus $K(P)$, cf. (2.2). The red dotted curve depicts the Murnaghan EoS stated at the beginning of Section 2.1. The residuals of the least-squares fit are depicted in the lower panel. Goodness-of-fit parameters are listed in Table 1. Parameters derived from the fit, the amplitudes a, b in EoS (2.1) and higher-order derivatives of K_0, are recorded in Table 2. (For interpretation of the colors in the figure(s), the reader is referred to the web version of this article.)

Table 3
One-parameter least-squares fit of the broken power-law EoS (2.1) with implemented Thomas-Fermi free-electron limit. The recorded parameters are described in the caption of Table 1, except that the exponent β is taken, like K_0 and K_0', as input parameter, so that the exponent η remains the only fitting parameter of the closed-form EoS in (2.1) and (2.5). The high-pressure limit of the EoS scales as $\rho(P) \propto P^\beta$, where the exponent β is identified with the scaling exponent $\beta = 3/5$ of a non-relativistic degenerate electron gas, cf. Section 2.2. The data sets used in the χ^2 functional (defined in the caption of Table 1) are the same as for the two-parameter fit in Fig. 1. This one-parameter fit of the copper EoS is depicted in Fig. 2 as red solid curve labeled '2' in the figure.

K_0 [GPa]	K_0'	β	η	χ^2	dof	SE	$1-R^2$
133.5	5.36	3/5	2.3923	3.481×10^{-3}	$116-1$	0.0203	3.41×10^{-4}

Table 4
One-parameter least-squares fit of the EoS (2.1), with implemented Thomas-Fermi limit and reduced data set. The regression is described in the caption of Table 3, the only difference being that the high-pressure data set obtained from DFT calculations is discarded in the χ^2 functional, namely the data points indicated by squares in Fig. 2. That is, only the empirical data points up to 450 GPa obtained by shockless compression [1] (circles in Figs. 1 and 2) are taken into account in the χ^2 fit. The listed input, fitting and goodness-of-fit parameters are described in the caption of Table 1. The regressed parameter is the exponent η. This least-squares fit is depicted in Fig. 2 as blue solid curve labeled '3.'

K_0 [GPa]	K_0'	β	η	χ^2	dof	SE	$1-R^2$
133.5	5.36	3/5	2.15455	6.30×10^{-5}	$84-1$	1.34×10^{-3}	3.80×10^{-5}

to obtain the values of the fitting parameters at the respective temperature T_n. Finally the parameters of EoS (2.1) are turned into smooth functions of temperature by performing a polynomial least-squares fit to each of the four data sets $a(T_n)$, $b(T_n)$, $\beta(T_n)$, $\eta(T_n)$. A similar method to empirically find the temperature dependence of fluid EoSs was used in Ref. [20]. Another option to extend the cold EoS (2.1) to high temperatures is to add the thermal pressure from a Debye model to the inverted EoS, cf. (3.1), and to specify a suitable density dependence of the Debye temperature, cf. Refs. [21–24].

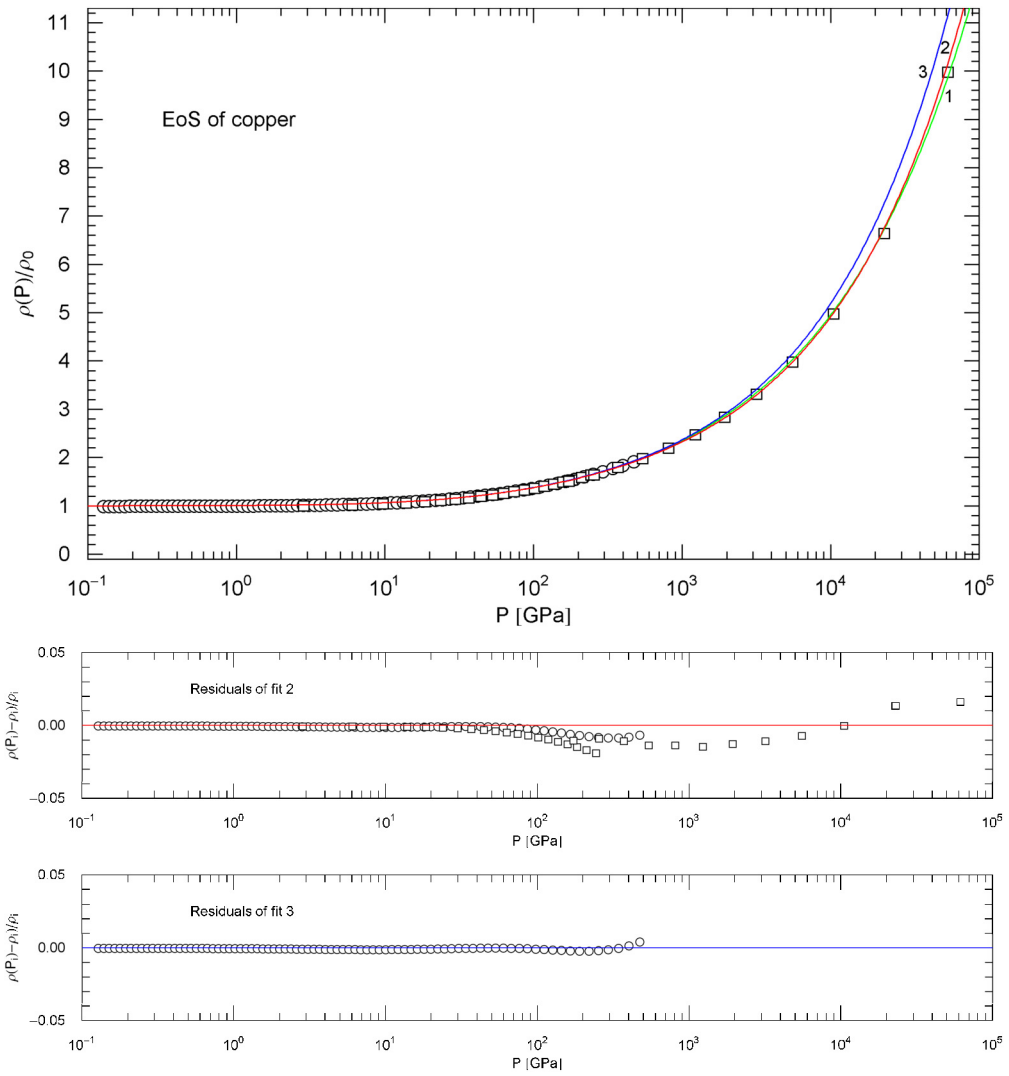

Fig. 2. EoS of copper in lin-log representation. Data points as in Fig. 1. The green curve (labeled '1') depicts the two-parameter fit (with exponents β, η as fitting parameters and K_0, K_0' as input) of the EoS in (2.1) and (2.5) as described in Fig. 1. The red curve (labeled '2') is a one-parameter fit to the same data set (with exponent η as fitting parameter and K_0, K_0' as input), assuming the Thomas-Fermi free-electron limit at ultra-high pressure, which requires the exponent $\beta = 3/5$, cf. Sections 2.2 and 5. The blue curve (labeled '3') is also a one-parameter (η) fit, but to the experimental data (circles) [1] only, without taking into account the high-pressure data points (squares) of the DFT calculation [2]. Residuals of the one-parameter fits are shown in the lower panels; residuals of the two-parameter fit (green curve) are indicated in Fig. 1. The fitting and goodness-of-fit parameters of the one-parameter fits are listed in Tables 3 and 4.

3. Relation of the broken power-law EoS to finite-strain equations of state

3.1. Low-pressure finite-strain epsilon expansion

The EoS (2.1) can be inverted in closed form to obtain pressure as a function of density,

$$P = b\big[(\rho/\rho_0)^{1/\eta}\big(1+(a/b)^{\beta/\eta}\big)-1\big]^{\eta/\beta} - a, \tag{3.1}$$

where ρ_0 is the density at zero pressure. For comparison, the Murnaghan EoS reads $P = (K_0/K_0')((\rho/\rho_0)^{K_0'}-1)$, cf. e.g. Refs. [25,26]. We define the epsilon expansion parameter $\varepsilon := (\rho/\rho_0)^{\alpha} - 1$, where the finite-strain exponent α can be positive or negative, and substitute $\rho/\rho_0 = (1+\varepsilon)^{1/\alpha}$ into EoS (3.1),

$$P(\varepsilon) = b\big[(1+\varepsilon)^{1/(\alpha\eta)}\big(1+(a/b)^{\beta/\eta}\big)-1\big]^{\eta/\beta} - a. \tag{3.2}$$

This equation is equivalent to EoS (3.1), which is independent of the finite-strain exponent α defining the expansion parameter ε. Eulerian strain requires the exponent $\alpha = 2/3$, Lagrangian strain $\alpha = -2/3$. Since $\rho > \rho_0$, ε is negative for negative α. We also eliminate the parameters a and b in (3.2) via (2.5) and (2.6), and finally perform the low-pressure ($|\varepsilon| << 1$) epsilon expansion of EoS (3.2),

$$P = \frac{1}{\alpha}K_0\varepsilon + \frac{K_0(K_0'-\alpha)}{2\alpha^2}\varepsilon^2 + c_3\varepsilon^3 + c_4\varepsilon^4 + \cdots, \tag{3.3}$$

where the parameter dependence of the indicated series coefficients is $c_3(\alpha;\beta,\eta;K_0,K_0')$ and $c_4(\alpha;\beta,\eta;K_0,K_0')$. We do not explicitly state these coefficients $c_{3,4}$ here, as they are lengthy expressions; in Mathematica®, the series (3.3) can readily be generated by expanding $P(\varepsilon)$ in (3.2) via FullSimplify[PowerExpand[Series[...]]].

By substituting $\beta(\eta;K_0,K_0',K_0'')$ (calculated in (2.8)) into the coefficient $c_3(\alpha;\beta,\eta;K_0,K_0')$, we obtain a handier expression in which the exponent η drops out,

$$c_3\big(\alpha;K_0,K_0'\big) = \frac{K_0}{6\alpha^3}\big(K_0'K_0' + K_0K_0'' - 3K_0'\alpha + 2\alpha^2\big). \tag{3.4}$$

Substitution of $\eta_\pm$ (calculated in (2.9)) and $\beta_\pm = \beta(\eta_\pm;K_0,K_0',K_0'')$ (cf. (2.8)) into the coefficient $c_4(\alpha;\beta,\eta;K_0,K_0')$ gives

$$c_4(\alpha; K_0, K_0') = \frac{K_0}{24\alpha^4}\big[K_0'^3 + 4K_0K_0'K_0'' + K_0^2K_0^{(3)} - 6\alpha\big(K_0'^2 + K_0K_0''\big) + 11K_0'\alpha^2 - 6\alpha^3\big], \tag{3.5}$$

which does not depend on the choice of sign in $\eta_\pm$, cf. (2.9).

To summarize, the finite-strain epsilon expansion of the EoS (3.1) reads

$$P = \frac{K_0\varepsilon}{\alpha}\bigg[1 + \frac{K_0' - \alpha}{2\alpha}\varepsilon + \frac{\alpha}{K_0}c_3(\alpha; K_0, K_0')\varepsilon^2 + \frac{\alpha}{K_0}c_4(\alpha; K_0, K_0')\varepsilon^3 + \cdots\bigg], \tag{3.6}$$

where $\varepsilon = (\rho/\rho_0)^\alpha - 1$, cf. (3.2), and the coefficients $c_{3,4}$ are stated in (3.4) and (3.5). The truncated power-series expansions (3.6) differ for different α. However, they are derived from one and the same EoS, namely (3.1), which is independent of the finite-strain exponent α defining the expansion parameter ε.

We briefly comment on the reasoning behind finite-strain expansions, cf. e.g. Refs. [27–30]. Assuming isotropic stress (hydrostatic pressure), as we do throughout this paper, a cube of initial side length a_0 gets compressed to a side length a, and we write $a - a_0 = h_E a$, where the contraction factor h_E is a negative constant, defined with respect to the compressed side length a. The volume compression is thus $V_0/V = (1-h_E)^3 = (1-2f_E)^{3/2}$, with finite-strain parameter $f_E := h_E - h_E^2/2$. Inversely, $f_E = (1-(V_0/V)^{2/3})/2$. This is the Eulerian definition of finite strain. The Lagrangian definition is based on $a - a_0 = h_L a_0$, where the contraction factor h_L refers to the initial side length a_0 of the cube. In this case, the volume contraction is $V/V_0 = (1+h_L)^3 = (1+2f_L)^{3/2}$, $f_L := h_L + h_L^2/2$, so that $f_L = ((V/V_0)^{2/3} - 1)/2$. Some authors define the finite-strain parameter with the opposite sign, to render f positive for compression [6]. Evidently, there is some arbitrariness in the definition of f as a function of V/V_0; the above definition of f_E and f_L is customary in elasticity theory, for isotropic strain.

Finite-strain equations of state, $P = -F_{,V}$, are obtained by assuming a truncated ascending series expansion for the free energy in terms of a finite-strain parameter, $F = \sum_{k=1}^N A_k f^k$, and by expressing the series coefficients A_k through the compression modulus and its derivatives $K_0^{(n)}$ at zero pressure, similarly as done in Section 2.1. Different choices of $f(V/V_0)$ in this truncated expansion will lead to different EoSs, and one can also try more general functions than f_E and f_L, so long as $f(V/V_0) \to 0$ for $V \to V_0$. There is, of course, no guarantee that one will obtain a viable EoS in this way. For instance, one can try linear combinations of f_E and f_L [27] or the generalized finite-strain parameter $f = -((V_0/V)^\alpha - 1)/(3\alpha)$, cf. Ref. [6], where α is a positive or negative exponent, so that $\alpha = \pm 2/3$ corresponds to Eulerian/Lagrangian strain, respectively. As the volume ratio V_0/V coincides with the density ratio ρ/ρ_0, we can write $f = -\varepsilon/(3\alpha)$, where $\varepsilon = (\rho/\rho_0)^\alpha - 1$ is the expansion parameter used in (3.3) and (3.6) and in the subsequent sections. Since the free energy F is defined from the outset as a (truncated) ascending series based on the assumption $|f| << 1$, finite-strain EoSs derived from it tend to fail at high density and pressure [18], cf. Section 4.2 for an explicit example of a finite-strain free-energy expansion.

3.2. Equivalence of the finite-strain epsilon expansion with the Birch-Murnaghan and Lagrangian EoSs

As mentioned in Section 3.1, finite-strain EoSs, such as the Birch-Murnaghan and Lagrangian EoSs, are customarily derived from a free energy functional assumed to be a truncated power series in the finite-strain parameter $f = -\varepsilon/(3\alpha)$, $\varepsilon = (\rho/\rho_0)^\alpha - 1$, with $\alpha = 2/3$ for the Birch-Murnaghan EoS and $\alpha = -2/3$ for the Lagrangian EoS, cf. e.g. Refs. [7,8,11,12,27–33]. (To save notation, we use ε instead of f as expansion parameter.) These EoSs are special cases of a generalized finite-strain EoS [6] that leaves the finite-strain exponent α unspecified (as a fitting parameter) and is defined by the truncated power series

$$P = \frac{K_0}{\alpha}(\rho/\rho_0)^{\alpha+1}\varepsilon\big(1 + a_1\varepsilon + a_2\varepsilon^2 + a_3\varepsilon^3 + \cdots\big), \tag{3.7}$$

with coefficients $a_1 = (K_0' - 3\alpha - 2)/(2\alpha)$ and

$$a_2 = \frac{1}{6\alpha^2}\big(K_0'K_0' + K_0K_0'' - 3K_0'(1+2\alpha) + 3 + 12\alpha + 11\alpha^2\big),$$
$$a_3 = \frac{1}{24\alpha^3}\big[K_0'^3 + K_0^2K_0^{(3)} + 4K_0K_0'K_0'' - \big(K_0'^2 + K_0K_0''\big)(4+10\alpha) + K_0'\big(6 + 30\alpha + 35\alpha^2\big) - \big(4 + 30\alpha + 70\alpha^2 + 50\alpha^3\big)\big]. \tag{3.8}$$

By putting $\alpha = 2/3$, one obtains the third-, fourth- and fifth-order Birch-Murnaghan equations, depending on how many terms are included in the series expansion. The n-th order EoSs (usually referred to in this way) are actually of order $n-1$ in epsilon, the third-order EoS being truncated after the $a_1\varepsilon$ term in (3.7), the fourth-order EoS after the $a_2\varepsilon^2$ term, etc. In contrast, the finite-strain expansion of the free energy (4.10) is in terms of $a_n\varepsilon^{n+2}$, so that the free energy of the fifth-order Birch-Murnaghan or Lagrangian EoS ($\alpha = -2/3$) is indeed of fifth order in ε.

The factor $(\rho/\rho_0)^{\alpha+1}$ in (3.7) is identical with $(1+\varepsilon)^{1+1/\alpha}$ (see after (3.1)), which is not expanded in (3.7). If we expand this factor as well in ε, the series expansions in (3.4)–(3.6) are recovered. Alternatively, we may write the EoS (3.1) or (3.2) as

$$P(\varepsilon) = \frac{(\rho/\rho_0)^{\alpha+1}}{(1+\varepsilon)^{1+1/\alpha}}\Big\{b\big[(1+\varepsilon)^{1/(\alpha\eta)}\big(1 + (a/b)^{\beta/\eta}\big) - 1\big]^{\eta/\beta} - a\Big\}, \tag{3.9}$$

where the factor in curly brackets admits the epsilon expansion stated in (3.4)–(3.6). If we also expand the denominator $(1+\varepsilon)^{1+1/\alpha}$ in (3.9), we recover the finite-strain EoS in (3.7) and (3.8). In brief, we have demonstrated that the fifth-order finite-strain expansion (3.7) is reproduced by the EoS (3.9). The latter, as emphasized after (3.6), is identical with our starting point, the EoS (3.1), which is independent of the finite-strain exponent α and also applies at high pressure. (The exponent α defines the expansion parameter $\varepsilon = (\rho/\rho_0)^\alpha - 1$ and the proportional finite-strain parameter $f = -\varepsilon/(3\alpha)$, cf. Section 3.1.)

The coincidence of the finite-strain expansion (3.7) with the epsilon expansion of EoS (3.9) terminates with the $a_3\varepsilon^3$ term in (3.7). Higher orders cannot be equivalent, since EoS (3.9) only depends on four parameters (a, b, β, η), whereas each additional term $a_n\varepsilon^n$ in (3.7) derived from finite-strain theory depends on a new parameter, namely the n-th derivative $K_0^{(n)}$ of the compression modulus at zero pressure. In practice, only the third- and fourth-order finite-strain EoSs, mainly Birch-Murnaghan with Eulerian strain exponent $\alpha = 2/3$, have been used when comparing with experimental data, cf. e.g. Refs. [34–38]. Here, we employ the closed-form EoS (2.1) for least-squares regression, cf. Section 2.2, instead of the finite-strain expansions (3.7), which are recovered in the low-pressure regime as demonstrated above.

Fig. 3 illustrates the (pressure) range of validity of the third-, fourth- and fifth-order Birch-Murnaghan and Lagrangian EoSs by comparing with high-pressure data sets of copper and with the regressed closed-form EoS (3.1) (using parameters a, b, β, η recorded in Tables 1 and 2). The series coefficients $a_{i=1,2,3}$ of the finite-strain expansions in (3.7) and (3.8) are listed in Table 5, calculated from the compression modulus and its derivatives $K_0^{(n=0,1,2,3)}$ in Tables 1 and 2. Since finite-strain expansions are ascending series

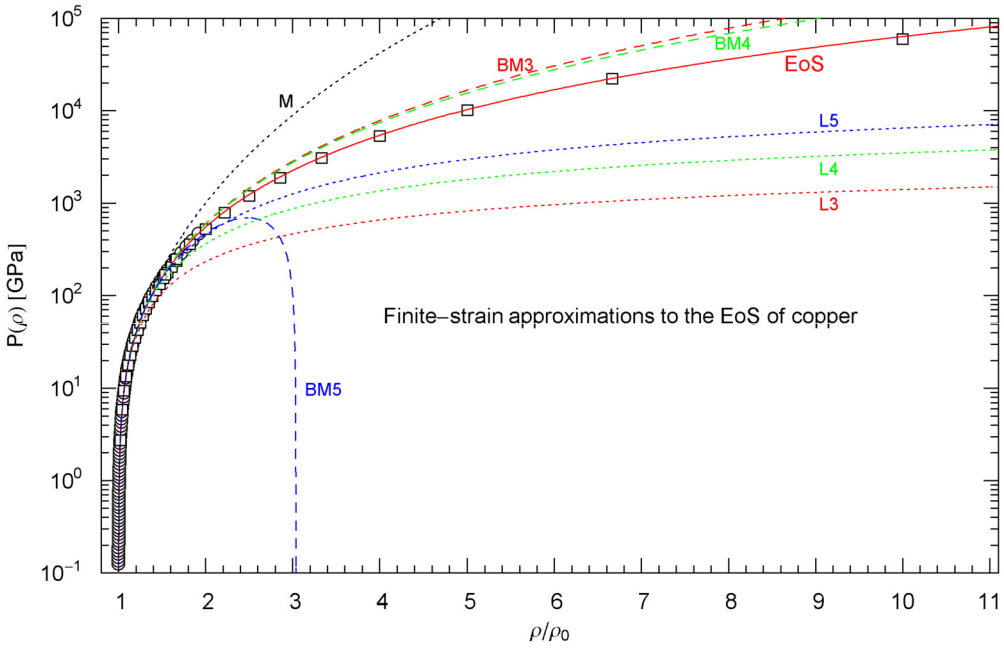

Fig. 3. Eulerian (Birch-Murnaghan) and Lagrangian finite-strain approximations to the high-pressure EoS of copper at ambient temperature. The closed-form EoS $P(\rho)$ in (3.1) is depicted as red solid curve (based on the least-squares fit in Fig. 1 and Tables 1 and 2). ρ_0 denotes the zero-pressure density of copper, cf. Table 2. The dotted black curve labeled 'M' indicates the Murnaghan EoS, cf. after (3.1), with K_0 and K_0' in Table 1. The dashed red, green and blue curves labeled 'BM3', 'BM4' and 'BM5' show the third-, fourth- and fifth-order Birch-Murnaghan EoSs, respectively, stated in (3.7) and (3.8), which are defined by the Eulerian finite-strain exponent $\alpha = 2/3$ and the compression modulus K_0 and its derivatives listed in Tables 1 and 2. The expansion coefficients $a_{i=1,2,3}$ of the EoSs in (3.8) are recorded (for copper) in Table 5. The dotted red, green and blue curves labeled 'L3', 'L4' and 'L5' show the third-, fourth- and fifth-order Lagrangian EoSs, also defined by the finite-strain expansions (3.7) and (3.8) but with exponent $\alpha = -2/3$, cf. Table 5. The finite-strain EoSs accurately fit the low-pressure data up to a few hundred GPa, but they are not suitable for the high-density regime, since they are ascending series expansions in $\varepsilon = (\rho/\rho_0)^\alpha - 1$ subject to $|\varepsilon| << 1$.

Table 5
Series coefficients of the third-, fourth- and fifth-order finite-strain expansions of the closed-form EoS (3.1) and free energy (4.2) of copper. The ascending series ε expansion is stated in (3.7) for the EoS and in (4.10) for the free energy. The finite-strain exponent α defines the expansion parameter $\varepsilon = (\rho/\rho_0)^\alpha - 1$, cf. Sections 3 and 4.2; ρ_0 denotes the zero-pressure density. The Birch-Murnaghan expansions depicted in Figs. 3 and 4 are obtained with the Eulerian finite-strain exponent $\alpha = 2/3$, and the Lagrangian expansions shown in these figures are defined by $\alpha = -2/3$. The listed expansion coefficients $a_i(\alpha)$ are calculated as stated in (3.8), depending on the compression modulus and its zero-pressure derivatives $K_0^{(n=0,1,2,3)}$ recorded in Tables 1 and 2 and based on the two-parameter χ^2 fit of the broken power-law EoS (2.1) in Fig. 1.

α	$a_1(\alpha)$	$a_2(\alpha)$	$a_3(\alpha)$
2/3	1.02	−0.05479	−1.556
−2/3	−4.02	10.025	−18.37

expansions in $\varepsilon = (\rho/\rho_0)^\alpha - 1$, based on the assumption $|\varepsilon| << 1$, it is not surprising that they fail at high pressure/density, but they are reasonably accurate up to pressures of a few hundred GPa, approximating the closed-form EoS (3.1). The latter has a well-defined high-pressure asymptotics and, more importantly, can be applied in the crossover regime (at TPa pressures), where the finite-strain expansion parameter is neither large nor small.

4. Free energy at ultra-high pressure and comparison with finite-strain theory

4.1. Closed-form expression of the free energy and high-pressure asymptotics

The free energy functional is obtained by integrating the broken power-law EoS $P(\rho)$ in (3.1), using $P = -F_{,V}$. Instead of volume, we use density as parameter, $\rho/\rho_0 = V_0/V$ (where the zero-subscripts indicate zero-pressure values) so that $P = F_{,\rho}\rho^2/(V_0\rho_0)$. As for the EoS in (3.1), we define the shortcut $\hat\rho_0 = (1 + (a/b)^{\beta/\eta})^{-\eta}\rho_0$ and write (3.1) as $P(\rho) = b((\rho/\hat\rho_0)^{1/\eta} - 1)^{\eta/\beta} - a$. The free energy then reads

$$\frac{F(\rho)}{V_0} = \rho_0 \int_{\hat\rho_0}^{\rho} \frac{P(\rho)}{\rho^2}\mathrm{d}\rho + c_F, \tag{4.1}$$

where c_F is an arbitrary integration constant independent of density ρ. Hence,

$$\frac{F(\rho)}{V_0} = \rho_0 b I_0(\rho) + \rho_0 a\left(\frac{1}{\rho} - \frac{1}{\hat\rho_0}\right) + c_F, \tag{4.2}$$

$$I_0(\rho) := \int_{\hat\rho_0}^{\rho} \left((\rho/\hat\rho_0)^{1/\eta} - 1\right)^{\eta/\beta}\frac{\mathrm{d}\rho}{\rho^2} = \frac{\eta}{\hat\rho_0}\int_0^{(\rho/\hat\rho_0)^{1/\eta}-1} x^{\eta/\beta}(x+1)^{-\eta-1}\mathrm{d}x, \tag{4.3}$$

where we used the variable transform $x = (\rho/\hat\rho_0)^{1/\eta} - 1$. F/V_0 is actually a function of ρ/ρ_0, and the zero-pressure density ρ_0, cf. Table 2, only enters via this ratio. Accordingly, when plotting F/V_0 against ρ/ρ_0, we do not even need to specify V_0 and ρ_0. Fig. 4 shows the plot of $(F(\rho) - F(\rho_0))/V_0$ for copper (with parameters a, b, β, η in Tables 1 and 2); the zero-pressure free energy density $F(\rho_0)/V_0$ is subtracted, so that the integration constant c_F in (4.1) drops out.

The second integral in (4.3) is a standard representation of a hypergeometric function,

$$I_0(\rho) = \frac{\eta}{\hat\rho_0}\frac{\beta}{\beta+\eta}\left((\rho/\hat\rho_0)^{1/\eta} - 1\right)^{1+\eta/\beta} \times {}_2F_1\left(1+\eta, 1+\eta/\beta; 2+\eta/\beta; -\left((\rho/\hat\rho_0)^{1/\eta} - 1\right)\right), \tag{4.4}$$

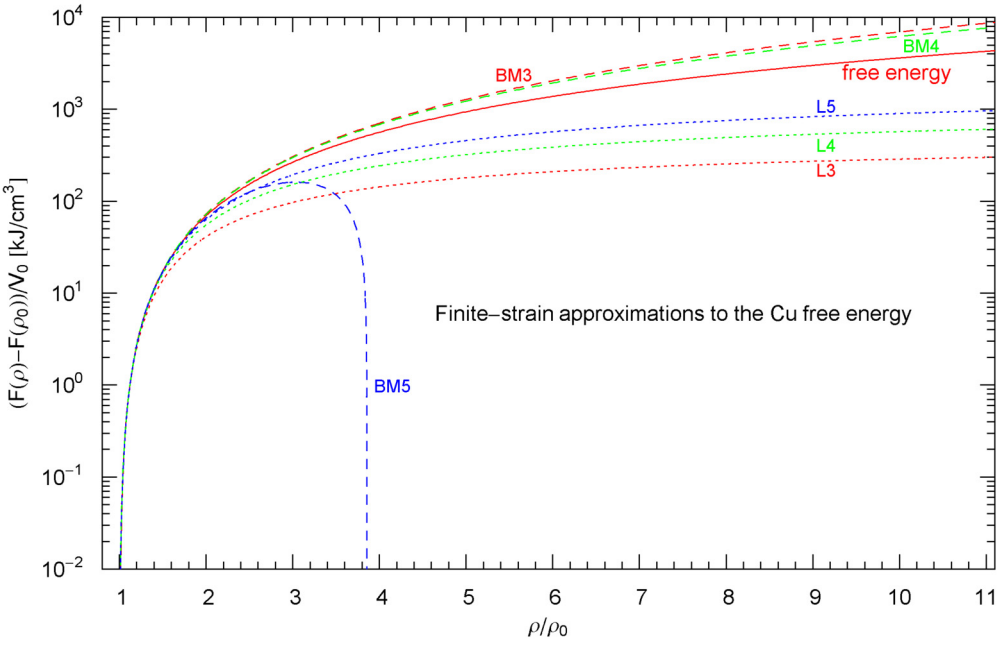

Fig. 4. Eulerian and Lagrangian finite-strain approximations to the free energy of copper, at ambient temperature. The red solid curve depicts the free energy density $F(\rho)/V_0$ in (4.2) and (4.4), obtained by integration of the high-pressure EoS (3.1) (with parameters in Tables 1 and 2). ρ_0 and V_0 denote density and volume at zero pressure; the zero-pressure free energy $F(\rho_0)$ is subtracted in the plot, cf. after (4.3) and (4.6). As for the units used, 1 GPa = 1 kJ/cm^3. The dashed red, green and blue curves labeled 'BM3', 'BM4' and 'BM5' show the free energies of the third-, fourth- and fifth-order Birch-Murnaghan EoSs, cf. Fig. 3, based on the finite-strain expansion (4.10) of the free energy with Eulerian finite-strain exponent $\alpha = 2/3$ and expansion coefficients $a_{i=1,2,3}$ in (3.8) and Table 5. The dotted red, green and blue curves labeled 'L3', 'L4' and 'L5' depict the free energies of the third- fourth- and fifth-order Lagrangian EoSs, also defined by the finite-strain expansion (4.10) with Lagrangian finite-strain exponent $\alpha = -2/3$, cf. Table 5 and Section 4.2. As in Fig. 3, the Eulerian expansions give slightly better approximations to the closed-form free energy (4.2) (red solid curve) at low and intermediate densities (as compared with the Lagrangian counterparts), but these ascending series expansions cannot be used at high pressure, irrespective of the choice of the finite-strain exponent α, in contrast to the free energy (4.2) derived from the closed-form EoS (3.1).

where $\rho/\hat\rho_0 = (1+(a/b)^{\beta/\eta})^\eta \rho/\rho_0$. This representation is efficient for low and intermediate pressure.

In the asymptotic high-density regime $\rho/\hat\rho_0 >> 1$, it is preferable to split the second integral in (4.3) as $\int_0^{(\rho/\hat\rho_0)^{1/\eta}-1} = \int_0^\infty - \int_{(\rho/\hat\rho_0)^{1/\eta}-1}^\infty$, where the first integral is a beta function and the second another representation of a hypergeometric function,

$$I_0(\rho) = \frac{\eta}{\hat\rho_0}\frac{\Gamma(\eta-\eta/\beta)\Gamma(1+\eta/\beta)}{\Gamma(1+\eta)} - \frac{\eta}{\hat\rho_0}\frac{1}{\eta-\eta/\beta}\big((\rho/\hat\rho_0)^{1/\eta}-1\big)^{\eta/\beta-\eta} \times {}_2F_1\big(1+\eta,\eta-\eta/\beta;1+\eta-\eta/\beta; -1/\big((\rho/\hat\rho_0)^{1/\eta}-1\big)\big). \tag{4.5}$$

The ascending series of ${}_2F_1$ can be substituted here to obtain the high-density asymptotic expansion. In any case, the closed-form expression of the free energy of EoS (3.1) is defined by (4.2) and (4.4) or (4.5). Singularities can emerge in (4.5) for special parameter values β and η, in which case one has to perform limit procedures in (4.5) or, preferably, recalculate integral (4.3) (which is always well-defined for positive parameters) with the respective special exponents. In leading order (in $\rho/\rho_0 >> 1$), the asymptotic EoS $P \propto \rho^{1/\beta}$ (see (2.10)) can be substituted into the integral (4.1) to find the high-pressure scaling $F \propto \rho^{1/\beta-1}$ for $\beta < 1$, $F \sim$ const for $\beta > 1$, and $F \propto \log(\rho/\rho_0)$ for $\beta = 1$.

4.2. Finite-strain low-density expansion of the free energy

To obtain the finite-strain expansion of the free energy in terms of $\varepsilon = (\rho/\rho_0)^\alpha - 1$, cf. Section 3.1, we start with $F(\rho)$ in (4.1) and split the integral there (taking note of $\hat\rho_0 < \rho_0$ since $\hat\rho_0 = (1+(a/b)^{\beta/\eta})^{-\eta}\rho_0$),

$$\frac{F}{V_0} = \rho_0\int_{\rho_0}^{\rho}\frac{P(\rho)}{\rho^2}\mathrm{d}\rho + d_F, \qquad d_F := \rho_0\int_{\hat\rho_0}^{\rho_0}\frac{P(\rho)}{\rho^2}\mathrm{d}\rho + c_F, \tag{4.6}$$

where d_F is a constant independent of density, and $P(\rho)$ is the EoS (3.1). The zero-pressure density ρ_0 drops out in d_F; the latter is calculated via $d_F = F(\rho_0)/V_0$ and (4.2) and (4.4). We can then write

$$\frac{F}{V_0} = \rho_0 I_1(\varepsilon) + d_F,$$

$$I_1 := \int_{\rho_0}^{\rho}\Big[b\big((\rho/\hat\rho_0)^{1/\eta}-1\big)^{\eta/\beta} - a\Big]\frac{\mathrm{d}\rho}{\rho^2} = \int_0^\varepsilon g(y)\mathrm{d}y,$$

$$g(y) := \frac{b[(1+y)^{1/(\alpha\eta)}(1+(a/b)^{\beta/\eta})-1]^{\eta/\beta} - a}{\rho_0\alpha(1+y)^{1/\alpha+1}}. \tag{4.7}$$

The variable transformation $y = (\rho/\rho_0)^\alpha - 1$ has been used here, so that the expansion parameter $\varepsilon = (\rho/\rho_0)^\alpha - 1$ appears as upper integration boundary. The finite-strain expansion of the free energy is found by expanding the integrand $g(y)$ in (4.7) in an ascending series in y and subsequent term-by-term integration. The free energy F in (4.7) is identical with (4.2) and is independent of the finite-strain exponent α defining the expansion parameter ε. As a consistency check, we note

$$P = -F_{,V} = \alpha(\rho/\rho_0)^{\alpha+1}F_{,\varepsilon}/V_0, \tag{4.8}$$

with $\rho/\rho_0 = V_0/V$ as in Section 4.1. Substitution of $F(\varepsilon)$ calculated in (4.7) reproduces the closed-form EoS (3.9).

The ascending series expansion of $g(y)$ in (4.7) is obtained by equating $P(\varepsilon)$ in (3.9) with P in (3.7) (and renaming ε there as y),

$$g(y) = \frac{K_0}{\rho_0\alpha^2}y\big(1+a_1y+a_2y^2+a_3y^3+\cdots\big), \tag{4.9}$$

with coefficients $a_{i=1,2,3}$ listed in (3.8). Term-by-term integration of the dy integral in (4.7) gives the finite-strain expansion of the free energy,

$$\frac{F}{V_0}=\frac{K_0}{\alpha^2}\left(\frac{1}{2}\varepsilon^2+\frac{a_1}{3}\varepsilon^3+\frac{a_2}{4}\varepsilon^4+\frac{a_3}{5}\varepsilon^5+\cdots\right)+d_F, \tag{4.10}$$

where $\varepsilon=(\rho/\rho_0)^\alpha-1$, and d_F is an integration constant, cf. (4.6). The coefficients $a_{i=1,2,3}$ are functions of the finite-strain exponent α and the compression modulus and its derivatives $K_0^{(n=0,1,2,3)}$ at zero pressure, explicitly given in (3.8). By substituting the expansion (4.10) into (4.8), the finite-strain ascending series expansion (3.7) of the EoS (3.1) is recovered. The finite-strain parameter $f=-\varepsilon/(3\alpha)$ can be used as expansion variable in (4.10) instead of ε, cf. Section 3.1.

In Fig. 4, finite-strain expansions of the free energy of copper are compared with the free energy derived from the high-pressure EoS (3.1), cf. Section 4.1. The closed-form free energy density $(F(\rho)-F(\rho_0))/V_0$ of copper is depicted in Fig. 4 as red solid curve, calculated by way of (4.2) and (4.4), with parameters a, b, β, η listed in Tables 1 and 2. The zero-pressure free energy $F(\rho_0)/V_0$ is subtracted, which is identical with the integration constant d_F in (4.6) and (4.10).

Also shown in Fig. 4 are the Eulerian ($\alpha=2/3$, corresponding to the Birch-Murnaghan EoS) and Lagrangian ($\alpha=-2/3$) finite-strain expansions of the free energy in (4.10) with series coefficients $a_{i=1,2,3}$ for copper listed in Table 5. The dashed curve in Fig. 4 labeled 'BM3' (third-order Birch-Murnaghan) is obtained by terminating the series expansion (4.10) after the ε^3 term, and the curves 'BM4' and 'BM5' by adding the fourth- and fifth-order terms. The Lagrangian finite-strain expansions are analogously labeled 'L3', 'L4', and 'L5' in this figure. The corresponding finite-strain EoSs are depicted in Fig. 3 (labeled in the same way) and can be recovered from the finite-strain expansion (4.10) of the free energy by differentiation, cf. (4.8). In the low-pressure range, the finite-strain expansions approximate the free energy density of copper based on the closed-form EoS (3.1) (solid red curve, cf. (4.2) and (4.4)) quite well, but they fail at high pressure, as do the finite-strain EoSs in Fig. 3.

5. Conclusion

The broken power-law EoS (2.1) is capable of modeling ultra-high pressure data sets, as demonstrated with copper compression data covering an extended pressure range up to 60 GPa, cf. Figs. 1 and 2 and Section 2.2. The inverted EoS (3.1) is also of closed form and admits a finite-strain ascending series expansion, which coincides with the third-, fourth- and fifth-order Birch-Murnaghan or Lagrangian EoSs, depending on the choice of the exponent α defining the finite-strain expansion parameter $f=-\varepsilon/(3\alpha)$, $\varepsilon=(\rho/\rho_0)^\alpha-1$, cf. Section 3. In Figs. 3 and 4, we determined the range of applicability of finite-strain expansions, which are accurate up to pressures of a few hundred GPa.

The proposed EoS (2.1) depends on four fitting parameters, two of which (the amplitudes a, b) can be replaced by the compression modulus at zero pressure K_0 and its first derivative K_0', cf. (2.5), usually determined by acoustic low-pressure experiments. Thus, by specifying K_0 and K_0' as experimental input, the EoS (2.1) only depends on the exponents β, η as fitting parameters, which were determined for copper by a least-squares fit depicted in Fig. 1. Based on this two-parameter fit, the high-pressure limit of the pressure derivative of the compression modulus, $K_\infty'=K'(P\to\infty)=1/\beta\approx 2.18$, is in accordance with the phenomenological bound $K_\infty'>5/3$ suggested in Refs. [18,19].

The EoS (2.1) admits a simple power-law $P\propto\rho^{1/\beta}$ as asymptotic high-pressure/high-density limit, cf. (2.10). Assuming the Thomas-Fermi free-electron limit $K_\infty'=5/3$ of a degenerate non-relativistic electron gas as ultra-high pressure limit (suggested in Ref. [6], in contrast to the bound $K_\infty'>5/3$) requires the exponent $\beta=3/5$, cf. Section 2.2, so that only the exponent η in EoS (2.1) remains as free fitting parameter to model the crossover to the ultra-high density regime. This possibility was explored in Fig. 2 and Tables 3 and 4, where we studied the crossover to the Thomas-Fermi limit, first by using the same data set as for the two-parameter fit in Fig. 1, and then with a reduced data set up to 450 GPa (based on shockless compression [1], discarding the ultra-high pressure data obtained from DFT calculations [2]).

By comparing the goodness-of-fit parameters of the three least-squares fits depicted in Figs. 1 and 2, we come to the conclusion that the assumption of the Thomas-Fermi free-electron limit as universal (i.e. material independent) ultra-high pressure limit remains a viable option, attractive because of its predictive power. In fact, as discussed in Section 2.2, it is possible to express the two amplitudes a, b and the exponent η in EoS (2.1) by the compression modulus and its first and second derivatives at zero pressure, $K_0^{(n=0,1,2)}$. These parameters can in principle be determined by low-pressure ultrasonic experiments, even though that is rarely done for the second derivative K_0'', cf. e.g. Refs. [27,39]. If we then use the exponent $\beta=3/5$ required by the Thomas-Fermi limit, the EoS (2.1) is completely determined by low-pressure experiments, in particular the crossover to the ultra-high pressure regime. This crossover is inaccessible by Eulerian (Birch-Murnaghan) or Lagrangian finite-strain expansions, as demonstrated in Figs. 3 and 4.

It becomes a matter of practical convenience whether to use a two-parameter (η,β) fit as done in Fig. 1 or a one-parameter fit by specifying the Thomas-Fermi limit $\beta=3/5$ in EoS (2.1). Currently, experimental data are usually only available for pressures well below 1 TPa, cf. e.g. Refs. [21–24,40–47]; at pressures above a few hundred GPa, Hugoniot shock compression is mostly employed [42,45]. For this reason, when extrapolating to ultra-high pressure, it is preferable to specify K_0 and K_0' (inferred from low-pressure ultrasonic measurements) as well as the Thomas-Fermi limit $\beta=3/5$ in EoS (2.1) (with amplitudes a, b in (2.5) substituted) and to determine the remaining parameter η in EoS (2.1) by least-squares regression from the available GPa data points, cf. Fig. 2 and Table 4.

The third- and fourth-order Birch-Murnaghan equations and the generalized Vinet equation [42,45] are arguably the most widely used phenomenological EoSs when performing least-squares fits to high-pressure data. These equations involve truncated series expansions, which tend to break down in the TPa pressure regime, cf. Fig. 3. Here, we have found a closed-form EoS, cf. (2.1) and (3.1), which amounts to a summation of finite-strain expansions up to the fifth order and is suitable for the crossover to ultra-high pressure. In case that discontinuities caused by structural transitions are perceptible in the data sets, one has to perform a separate fit of the EoS in each pressure interval defined by the discontinuities. And even if pressure-induced transitions cannot be identified, be it because the available data sets do not extend to pressures where they occur or because the discontinuities are not sufficiently pronounced relative to the scatter in the data, one can still obtain an estimate of the pressure-density relation at ultra-high pressure by implementing the Thomas-Fermi free-electron limit into the EoS, as done in Section 2.2.

Declaration of competing interest

The author declares that he has no known competing financial interests or personal relationships that could have appeared to influence the work reported in this paper.

References

[1] R.G. Kraus, J.-P. Davis, C.T. Seagle, D.E. Fratanduono, D.C. Swift, J.L. Brown, J.H. Eggert, Phys. Rev. B 93 (2016) 134105.
[2] C.W. Greeff, J.C. Boettger, M.J. Graf, J.D. Johnson, J. Phys. Chem. Solids 67 (2006) 2033.
[3] W.B. Holzapfel, High Press. Res. 30 (2010) 372.
[4] A. Dewaele, P. Loubeyre, M. Mezouar, Phys. Rev. B 70 (2004) 094112.
[5] P.I. Dorogokupets, A.R. Oganov, Phys. Rev. B 75 (2007) 024115.
[6] W.B. Holzapfel, Rep. Prog. Phys. 59 (1996) 29.
[7] F.D. Stacey, Phys. Earth Planet. Inter. 128 (2001) 179.
[8] K. Sushil, K. Arunesh, P.K. Singh, B.S. Sharma, Physica B 352 (2004) 134.
[9] J. Hama, K. Suito, J. Phys. Condens. Matter 8 (1996) 67.
[10] F.D. Stacey, Rep. Prog. Phys. 68 (2005) 341.
[11] W.B. Holzapfel, Z. Kristallogr. 216 (2001) 473.
[12] W.B. Holzapfel, High Press. Res. 16 (1998) 81.
[13] F.D. Stacey, J.H. Hodgkinson, Phys. Earth Planet. Inter. 286 (2019) 42.
[14] R. Tomaschitz, Physica B 593 (2020) 412243.
[15] R. Tomaschitz, J. Phys. Chem. Solids 152 (2021) 109773.
[16] R. Tomaschitz, Physica A 541 (2020) 123188.
[17] J.R. Macdonald, Rev. Mod. Phys. 38 (1966) 669.
[18] F.D. Stacey, P.M. Davis, Phys. Earth Planet. Inter. 142 (2004) 137.
[19] F.D. Stacey, Geophys. J. Int. 143 (2000) 621.
[20] R. Tomaschitz, Fluid Phase Equilib. 496 (2019) 80.
[21] S. Speziale, C.-S. Zha, T.S. Duffy, R.J. Hemley, H.-K. Mao, J. Geophys. Res., Solid Earth 106 (2001) 515.
[22] T. Sakai, S. Takahashi, N. Nishitani, I. Mashino, E. Ohtani, N. Hirao, Phys. Earth Planet. Inter. 228 (2014) 114.
[23] P.I. Dorogokupets, A.M. Dymshits, K.D. Litasov, T.S. Sokolova, Sci. Rep. 7 (2017) 41863.
[24] F. Miozzi, J. Matas, N. Guignot, J. Badro, J. Siebert, G. Fiquet, Minerals 10 (2020) 100.
[25] W.B. Holzapfel, High Press. Res. 22 (2002) 209.
[26] R. Tomaschitz, Appl. Phys. A 126 (2020) 102.
[27] O.L. Anderson, Equations of State of Solids for Geophysics and Ceramic Science, Oxford University Press, New York, 1995.
[28] F.D. Stacey, B.J. Brennan, R.D. Irvine, Geophys. Surv. 4 (1981) 189.
[29] L. Thomsen, J. Phys. Chem. Solids 31 (1970) 2003.
[30] T. Katsura, Y. Tange, Minerals 9 (2019) 745.
[31] B.L.N. Kennett, Phys. Earth Planet. Inter. 307 (2020) 106558.
[32] R.E. Cohen, O. Gülseren, R.J. Hemley, Am. Mineral. 85 (2000) 338.
[33] S.K. Sikka, Phys. Lett. A 135 (1989) 129.
[34] D.M. Hoat, Phys. Lett. A 383 (2019) 1648.
[35] D.M. Hoat, N.H. Giang, M. Naseri, R. Ponce-Pérez, J.F. Rivas-Silva, G.H. Cocoletzi, Phys. Lett. A 384 (2020) 126589.
[36] K. Fuchizaki, K. Okamoto, Phys. Lett. A 380 (2016) 293.
[37] Z.-W. Niu, M. Tang, L.-C. Cai, Phys. Lett. A 384 (2020) 126598.
[38] Y.-L. Jiang, Y.-Z. Chen, H. Wang, X.-B. Yang, Phys. Lett. A 384 (2020) 126658.
[39] M. Matsui, Y. Higo, Y. Okamoto, T. Irifune, K.-I. Funakoshi, Am. Mineral. 97 (2012) 1670.
[40] C.-S. Zha, H.K. Mao, R.J. Hemley, Proc. Natl. Acad. Sci. USA 97 (2000) 13494.
[41] T. Uchida, Y. Wang, M.L. Rivers, S.R. Sutton, J. Geophys. Res., Solid Earth 106 (2001) 799.
[42] Y. Wang, R. Ahuja, B. Johansson, J. Appl. Phys. 92 (2002) 6616.
[43] W.J. Panero, L.R. Benedetti, R. Jeanloz, J. Geophys. Res., Solid Earth 108 (2003) 2015.
[44] J.-F. Lin, A.J. Campbell, D.L. Heinz, J. Geophys. Res., Solid Earth 108 (2003) 2045.
[45] A.D. Chijioke, W.J. Nellis, I.F. Silvera, J. Appl. Phys. 98 (2005) 073526.
[46] Y. Fei, A. Ricolleau, M. Frank, K. Mibe, G. Shen, V. Prakapenka, Proc. Natl. Acad. Sci. USA 104 (2007) 9182.
[47] Y. Fei, C. Murphy, Y. Shibazaki, A. Shahar, H. Huang, Geophys. Res. Lett. 43 (2016) 6837.